Asian Journal of Chemistry; Vol. 38, No. 4 (2026), 863-870
ASIAN JOURNAL OF CHEMISTRY
https://doi.org/10.14233/ajchem.2026.35275

Design, Synthesis and *in silico* Studies of Pyrazoline-based Compounds as Anticancer Inhibitors

KUMUD P. BHENDARKAR[1,*], DEEPALI M. WANODE[1] and PRAMOD B. KHEDEKAR[2]

[1]Department of Pharmaceutical Sciences, Rashtrasant Tukadoji Maharaj Nagpur University, Nagpur-440033, India
[2]Nagpur College of Pharmacy, Wanadongari, Hingna Road, Nagpur-441110, India

*Corresponding author: E-mail: kumud.mendhe123@gmail.com

Received: 17 November 2025 *Accepted*: 21 January 2026 *Published online*: 8 April 2026 AJC-22306

In this work, few new pyrazoline derivatives **Py1-Py5** were synthesised, characterised and their potential as EGFR kinase inhibitors was assessed. The target compounds were synthesized *via* Claisen-Schmidt condensation, followed by cyclization of the resulting chalcones using thiosemicarbazide. The anticipated chemical frameworks were confirmed by structural elucidation utilizing IR, ^{1}H NMR, ^{13}C NMR and HRMS studies. All the derivatives showed substantial binding affinities in molecular docking analysis using AutoDock Vina against EGFR kinase (PDB ID: 3POZ). Compound **Py3** exhibited the highest docking score (-10.2 kcal/mol), surpassing the co-crystallized ligand O3P (-10.0 kcal/mol) and demonstrated interactions with key EGFR inhibitory residues, including Lys50, Thr95, Met98 and Val131. ADMET projections indicated low toxicity, excellent pharmacokinetic characteristics and synthetic accessibility. Furthermore, compound **Py2** had the lowest IC_{50} value (44.47 µg/mL) in an *in vitro* cytotoxicity screening against MCF-7 breast cancer cells using the MTT test, indicating considerable activity. The structure-activity relationship analysis suggested that the presence of electron withdrawing substituents, especially chloro and nitro groups, enhances the cytotoxicity activity.

Keywords: Pyrazoline derivatives, EGFR kinase, Molecular docking, ADMET, Cytotoxicity, MCF-7 cells.

INTRODUCTION

The broad spectrum of biological potential heterocyclic compounds makes them an important component of medicinal chemistry [1]. The versatility and great biological potential of nitrogen-containing heterocycles have aroused the curiosity of numerous researchers in recent years. The basic character of pyrazolone is attributed to the nitrogen atoms present in its five-membered heterocyclic ring, which can readily accept protons [2,3]. Pyrazoline, a partially saturated derivative of pyrazole containing an endocyclic double bond, is another important heterocyclic scaffold, with 2-pyrazoline being the most extensively studied because of its greater stability [4]. Chalcones play a significant role in organic synthesis and industrial applications, serving as key intermediates in the preparation of various heterocyclic compounds, including pyrazoline derivatives [5-8].

Cancer is one of the most serious health challenges worldwide and remains a major cause of mortality [9]. It comprises more than 100 distinct diseases which are generally classified based on the organ or tissue in which they originate. Among women, the most frequently diagnosed cancers include breast, lung, uterine, colorectal and thyroid cancers, whereas prostate, lung, colorectal and bladder cancers are commonly reported among men. Globally, prostate cancer in men and breast cancer in women are among the most prevalent forms of the disease [10]. Reports from the International Agency for Research on Cancer (IARC) of the World Health Organization (WHO) indicate that lung cancer accounts for approximately 2.5 million new cases each year, followed by female breast cancer with around 2.3 million cases. Lung cancer also represents the leading cause of cancer-related deaths, while breast cancer remains one of the major contributors to global cancer mortality [11,12].

A variety of therapeutic approaches have been developed for the management of cancer, with chemotherapy being one of the most commonly employed treatments. Chemotherapy involves the use of powerful chemical agents that primarily target rapidly dividing cells, thereby inhibiting the growth of cancer cells that proliferate more quickly than normal cells [13,14]. Despite its effectiveness, chemotherapy is associated with several drawbacks including lack of selectivity, systemic toxicity, development of drug resistance and damage to healthy tissues, all of which can adversely affect patients'

quality of life. These limitations have encouraged ongoing efforts to identify safer and more targeted anticancer therapies. In this regard, tyrosine kinase inhibitors have emerged as promising therapeutic agents for cancer treatment [15,16]. The epidermal growth factor receptor (EGFR) family, which includes EGFR (ErbB1), HER2 (ErbB2), HER3 (ErbB3) and HER4 (ErbB4), belongs to the receptor tyrosine kinase group and plays a key role in regulating essential cellular functions such as proliferation, differentiation, metabolism and survival [17-19]. Activation of these receptors occurs when specific ligands bind to the extracellular domain, resulting in receptor dimerisation and phosphorylation of the intracellular tyrosine kinase domain, which subsequently activates several downstream signalling pathways [20-23].

Based on these facts, an attempt was made to synthesise and investigate new pyrazoline-based derivatives as potential anticancer agents targeting the epidermal growth factor receptor (EGFR) kinase. The synthesized compounds were characterised using spectroscopic methods and evaluated through the molecular docking to examine their interaction with the EGFR active site. In addition, their cytotoxic potential against MCF-7 breast cancer cells was assessed along with ADMET predictions to identify compounds with promising biological activity and favourable pharmacokinetic properties.

EXPERIMENTAL

All reagents were purchased from commercial suppliers. The melting points were determined using an Equiptronics digital melting point device and are uncorrected. IR spectra were recorded using on Shimadzu FTIR in the 4000-400 cm^{-1} range. ^1H NMR & ^{13}C NMR spectra were recorded on a BRUKER AVANCE NEO 500 MHz NMR spectrophotometer in $CDCl_3$ and DMSO, respectively as solvent. Mass spectra were recorded using a TOF MS ES model. The progress of the reaction was tracked by using thin-layer chromatography (TLC) on TLC silica gel 60 F_{254} aluminium sheets using ethyl acetate:*n*-hexane (9:1 v/v) as eluent.

Synthesis of chalcones (Cha1-Cha5): 3-Acetylcoumarin (**1**, 2 mmol) dissolved in ethanol was mixed with KOH solution and stirred at room temperature followed by the addition of substituted benzaldehyde (**2**, 2 mmol) after 0.5 h. The mixture was stirred continuously for a further 24 h. Using a 9:1 ethyl acetate:*n*-hexane solvent solution, the progress of the reaction through TLC was monitored. After completion, the mixture was neutralised with dilute HCl and quenched with crushed ice (**Scheme-I**) [24,25]. The resulting residue was collected by filtration and the product was recrystallisation in ethanol to afford **Cha1-Cha5** as a pale-yellow solid in 42-68% yield.

Synthesis of pyrazoline derivatives (Py1-Py5): A mixture of thiosemicarbazide (0.01 mol, 0.91 g), substituted chalcones (**Cha1-Cha5**) (0.01 mol) and a catalytic quantity of HCl (1 mL) was refluxed in 30 mL of ethanol for 6-8 h. Following cooling, the formed precipitate was filtered, washed with water, dried and then recrystallised from ethanol.

5-(2-Chlorophenyl)-3-(2-oxo-2*H*-1-benzopyran-3-yl)-4,5-dihydro-1*H*-pyrazole-1-carbothioamide (Py1): Yield: 68%, m.p.: 169-172 ºC, m.f.: $C_{19}H_{14}N_3O_2SCl$ (m.w. 355.18); IR (KBr, ν_{max}, cm^{-1}): 3368.74, 3261.04 (N–H), 3174.88 (C–H *str*. arom.), 1286.51 (C=S), 1161.68 (C–O–C), 772.54 (C–Cl); ^1H NMR (500 MHz, $CDCl_3$, δ ppm): 3.90 (s, 2H), 5.19 (s, 2H), 7.26 (s, 1H), 7.40 (d, 1H), 7.53 (t, 1H), 7.63 (t, 1H), 8.01 (d, 1H), 8.07 (d, 1H); ^{13}C NMR (500 MHz, DMSO, δ ppm): 195.56, 159.28, 155.36, 147.52, 134.43, 130.25, 125.01, 124.55, 121.00, 118.28, 116.73; HR-MS: *m/z* 356.09.

5-(2-Chloro-5-nitro-phenyl)-3-(2-oxo-2*H*-1-benzopyran-3-yl)-4,5-dihydro-1*H*-pyrazole-1-carbothioamide (Py2): Yield: 42%, m.p.: 172-178 ºC, m.f.: $C_{19}H_{13}N_4O_4SCl$ (m.w. 428.8); IR (KBr, ν_{max}, cm^{-1}): 3439.10, 3315.61 (N–H), 3170.58 (C–H *str*. arom.), 1266.07 (C=S), 1108.55 (C–O–C), 751.00 (C–Cl); ^1H NMR (500 MHz, $CDCl_3$, δ ppm): 3.89 (s, 2H), 6.90 (m, 2H), 7.30 (t, 1H), 7.40 (d, 1H), 7.74 (t, 1H), 7.85 (d, 1H), 7.26 (d, 1H), 8.20 (dd, 1H); ^{13}C NMR (500 MHz, DMSO, δ ppm): 194.96, 156.31, 154.49, 146.91, 134.35, 130.65, 124.61, 118.05, 115.99; HR-MS: *m/z* 428.28.

5-(4-Hydroxy-3,5-dimethyl-phenyl)-3-(2-oxo-2*H*-1-benzopyran-3-yl)-4,5-dihydro-1*H*-pyrazole-1-carbothioamide (Py3): Yield: 58%, m.p.: 170-182 ºC; m.f.: $C_{21}H_{19}N_3O_3S$ (m.w. 393.46); IR (KBr, ν_{max}, cm^{-1}): 3410.38, 3285.45 (N–H), 3169.14 (C–H *str*. arom.), 1266.1 (C=S), 1158.81 (C–O–C); ^1H NMR (500 MHz, DMSO, δ ppm): 2.50 (s, 6H), 3.31 (s, 2H), 6.71 (d, 3H), 7.40 (m, 1H), 7.30-7.60 (t, 1H), 7.96 (d, 1H), 8.66 (d, 1H), 9.30 (s, 1H), 11.23 (s, 1H); ^{13}C NMR (500 MHz, DMSO, δ ppm): 190.28, 158.31, 154.49, 146.91, 134.35, 130.49, 126.57, 124.30, 124.09, 118.0, 115.9, 29.70, 15.17; HR-MS: *m/z* 394.10.

5-(3,4,5-Trimethoxyphenyl)-3-(2-oxo-2*H*-1-benzopyran-3-yl)-4,5-dihydro-1*H*-pyrazole-1-carbothioamide (Py4): Yield: 45%, m.p.: 110-115 ºC, m.f.: $C_{22}H_{21}N_3O_5S$ (m.w. 439.49); IR (KBr, ν_{max}, cm^{-1}): 3294.07, 3192.11 (N–H), 2996 (C–H *str*. arom.), 1272 (C=S), 1121.48 (C–O–C); ^1H NMR (500 MHz, $CDCl_3$, δ ppm): 3.81 (dd, 1H), 3.85-3.95 (m, 9H), 6.73 (d, 1H), 6.90 (d, 2H), 7.25-7.41 (2H), 7.61-8.07 (s, 3H), 9.98 (s, 1H); ^{13}C NMR (500 MHz, DMSO, δ ppm): 161.8, 156.7, 154.3, 145.3, 141.9, 131.3, 128.0, 125.7, 122.6, 117.8, 116.6, 125.7, 122.6, 117.8, 116.6, 111.8, 61.1, 59.1, 56.3, 41.8, 61.1, 59.1, 56.3, 41.8. HRMS: *m/z* 438.19.

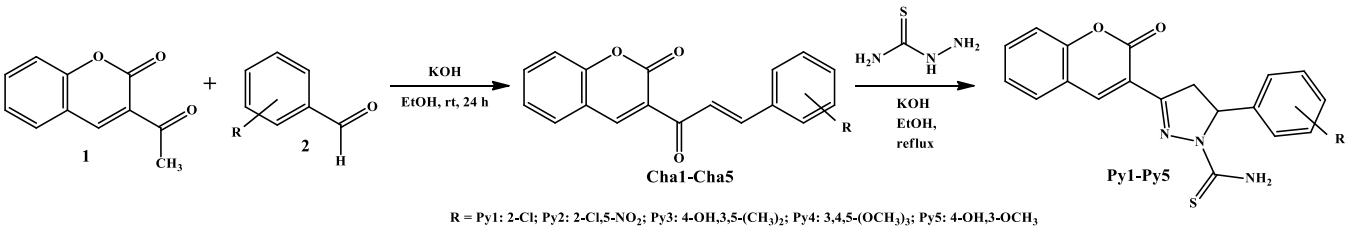

Scheme-I: Synthetic route of pyrazolines (**Py1-Py5**)

5-(4-Hydroxy-3-methoxy-phenyl)-3-(2-oxo-2*H*-1-benzopyran-3-yl)-4,5-dihydro-1*H*-pyrazole-1-carbothioamide (Py5): Yield: 42%, m.p.: 140-144 ºC, m.f.: $C_{20}H_{17}N_3O_4S$ (*m.w.* 395.5); IR (KBr, ν_{max}, cm^{-1}): 3367.30, 3259.60 (N–H), 3174.88 (C–H *str*. arom.), 1285.87 (C=S), 1161.68 (C–O–C); ^{1}H NMR (500 MHz, $CDCl_3$, δ ppm): 3.57 (dd, 1H), 3.77 (s, 3H), 3.97 (dd, 1H), 6.71 (dd, , 1H), 7.63-7.26 (m, 7H), 8.07 (d, 1H), 9.18-9.05 (s, 2H), 11.39 (s, 1H); ^{13}C NMR (500 MHz, DMSO, δ ppm): 163.6, 160.9, 153.3, 152.1, 141.9, 130.3, 128.4, 126.7, 122.2, 118.8, 116.4, 115.5, 109.2, 60.0, 55.3, 40.4; HRMS: *m/z* 396.13.

In silico and molecular docking studies

Molecular docking studies: To investigate the molecular docking investigations, AutoDock Tools software (Version 1.5.7) was used. An open-source, grid-based molecular interaction tool called AutoDock Vina (ADV) was used to forecast the best non-covalent binding conformations between the ligand and the macromolecular receptor. This tool uses an effective scoring and search algorithm to improve the accuracy of binding mode predictions. ChemDraw 16.0 was used to sketch the targeted ligands, the Protein Data Bank was used to retrieve the protein EGFR kinase and PyMOL Visualizer was used to visualize and interpret the docking results. To ensure full coverage of the active site, the grid box was adjusted to dimensions of 17.05 × 33.038 × 13.333 $Å^3$ for the docking technique. The grid center coordinates were defined as x = 40, y = 40 and z = 40 Å. Based on the target protein's binding site for the co-crystallised ligand, these characteristics were ascertained visually. In order to confirm the specificity of the binding site and assess the docking protocol, the co-crystallized ligand, *N*-{2-[4-({3-chloro-4-[3-(trifluoromethyl)-phenoxy]phenyl}amino)-5*H*-pyrrolo[3,2-*d*]pyrimidin-5-yl]-ethyl}-3-hydroxy-3-methylbutanamide, was re-docked into the active site, and its resulting conformation was compared with the original crystallographic pose. Moreover, the PLIP web-based program was used to examine the detailed protein-ligand interaction modes for each complex [26].

Ligand preparation: The ligands used for the molecular docking study were initially sketched using ChemDraw software (Fig. 1) and their structures were cleaned and corrected for proper bond alignment. Each ligand molecule was given 3D conformations after hydrogen atoms were added by the normal ligand synthesis procedure. Partial charges were also allocated and the pH was changed to 7.2 to correspond with physiological conditions. These changes guaranteed the ligands' precise electrical characteristics and shape, which are necessary for docking simulations. Afterwards, every produced ligand was transformed and stored in the ".pdbqt" format, which is the required AutoDock Vina (ADV) input file type. The PDBQT format contains important chemical information that isn't included in regular PDB files, like AutoDock-specific atom types (T) and partial charges (Q). These atom types improve the accuracy of docking predictions by enabling a more accurate representation of molecular characteristics, such as the distinction between aliphatic and aromatic carbons. Reliable molecular interactions during the docking process depend on the creation of PDBQT files with the correct shape, charge and atom-type information [27,28].

Protein preparation: Utilizing AutoDock Tools (ADT) [29], the protein structure utilised for the molecular docking investigation was created by AutoDock Vina's normal procedure. The protein data bank provided the crystal structure of EGFR kinase (PDB ID: 3POZ). Ligand *N*-{2-[4-({3-chloro-4-[3-(trifluoromethyl)phenoxy]phenyl}amino)-5*H*-pyrrolo-[3,2-*d*]pyrimidin-5-yl]ethyl}-3-hydroxy-3-methylbutanamide co-crystallizes with this structure, which was determined by X-ray diffraction at a high resolution of 1.50 Å. PyMOL was used for the protein's first processing and visualisation [30]. In the preparation process, the co-crystallised ligand, water molecules and any undesirable heteroatoms were eliminated. Homology modeling was used to adjust for any missing side

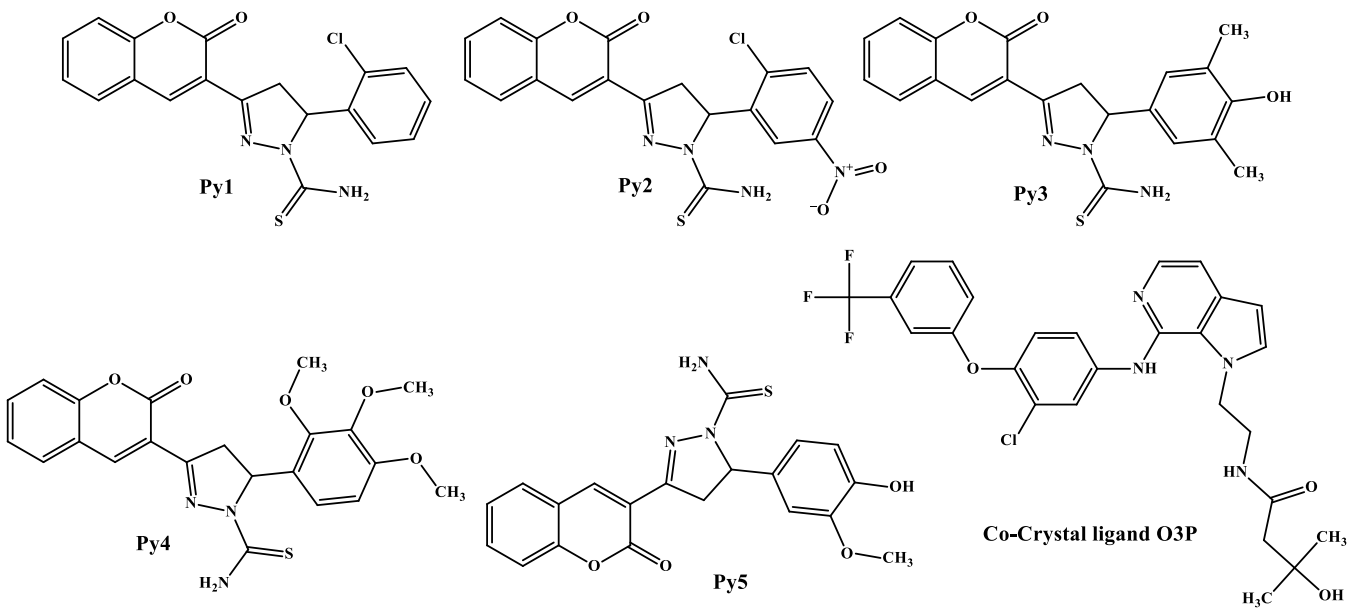

Fig. 1. 2D structures of synthesised **Py1**-**Py5** compound and co-crystal ligand O3P

chains and residues. A thorough analysis of the protein revealed structural anomalies that required remedial action, such as missing loops. The protein was homologously modeled using the SWISS-MODEL service to rectify these anomalies [31]. Pymol visualisation software was then used to compare the modelled protein to the original co-crystallised O3P protein on several criteria. The reduced protein was then loaded into AutoDock Tools, where Gasteiger charges and polar hydrogen atoms were added. The AMBER force field (FF) was then used to minimize energy in the protein to minimize steric conflicts and optimize the structure. The final receptor structure was saved in the .pdbqt format for docking and the atom types were determined using the AutoDock4 format [32,33].

Before screening a molecular database, the docking protocol must be validated. This was achieved through self-docking, where the co-crystallized ligand was redrawn and docked into the same binding site to verify whether a similar orientation could be reproduced. The co-crystal ligand N-{2-[4-({3-chloro-4-[3-(trifluoromethyl)phenoxy]phenyl}amino] was re-docked, and the superimposition using PyMol yielded an RMSD value of 0.678 Å (Fig. 2). Since an RMSD value below 2 Å indicates reliable docking accuracy, the protocol was considered valid. The binding energy of the co-crystal ligand was -10 kcal/mol, which was used as the reference threshold for further molecular screening [34].

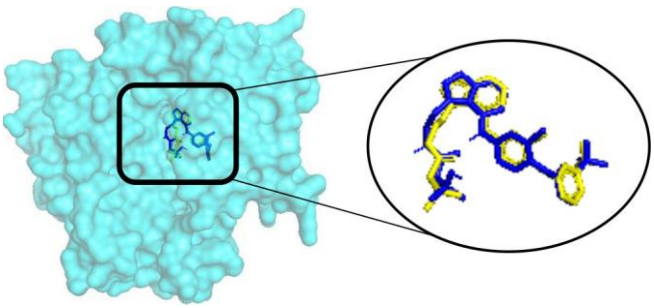

Fig. 2. Redocking of co-crystal ligand

Prediction of synthetic accessibility and toxicity: To determine whether the selected new compounds are drug-like and suitable for further development, their synthetic accessibility and toxicity profiles were analysed. The SwissADME web tool was used to predict the synthetic accessibility (SA) of the compounds. The SA values range from 1 to 10, with a lower number indicating easier synthesis. Compounds that were considered synthetically feasible and selected for further investigation had SA values less than 5 [35]. The ADMETAI tool, which uses a machine-learning algorithm based on molecular fingerprints to predict various toxicity characteristics, was used to assess the toxicity. In addition, the compounds showed adequate skin permeability, blood-brain barrier (BBB) penetration, intestinal absorption and central nervous system (CNS) permeability. All compounds were within safe limits and show no toxicity concerns, including AMES mutagenicity, maximum tolerated dose, hepatotoxicity, skin sensitisation or minnow toxicity. According to these results, the selected compounds have good pharmacokinetic, toxicological and synthetic accessibility characteristics, making them attractive options for further research [36,37].

***In vitro* cytotoxicity studies:** The MTT assay was used to evaluate the cytotoxic potential of synthetic pyrazoline derivatives on human breast cancer cells, MCF-7. The cells from NCCS, Pune, India were cultivated in minimum essential medium (MEM) with the addition of 10% FBS and maintained at 37 ºC and 5% CO_2. Approximately 1×10^4 cells per well were seeded in 96-well plates and the test drugs were added at doses between 10 and 100 µg/mL. A 0.2% DMSO in PBS was added to the control wells. Each treatment was performed in triplicate. After 24 h, 20 µL of MTT solution (5 mg/mL) was added and the mixture was incubated for 4 h. After a 10 min incubation, 200 µ L of DMSO was used to dissolve the formazan crystals produced by the live cells on the plates. The absorbance at 570 nm was measured using an ELISA reader (Benephera E21). To calculate the IC_{50} values, cell viability (%) was compared with the control [38].

RESULTS AND DISCUSSION

The pyrazoline derivatives (**Py1-Py5**) were obtained through cyclization of the previously synthesized chalcones (**Cha1-Cha5**) with thiosemicarbazide in ethanol under reflux in acidic conditions. This transformation involves nucleophilic addition of thiosemicarbazide to the β-unsaturated carbonyl system of chalcone, followed by intramolecular ring closure to form the pyrazoline framework. The reactions proceeded efficiently and produced the target compounds in moderate yields ranging from 42% to 68%. The physical characterisation further supported the successful synthesis of the derivatives. For instance, compound **Py1** exhibited a melting point in the range of 187-195 ºC, indicating good purity and crystallinity. In the IR spectra, the coumarin moiety showed characteristic C–O–C stretching vibrations, along with N–H stretching bands around 3400-3200 cm^{-1} and thioamide (C=S) absorptions at 1286-1260 cm^{-1}. In the ^1H NMR spectra, the methine proton of the pyrazoline ring appeared at δ 5.5-5.9 ppm, while the methylene protons appeared as doublets of doublets between δ 3.1-3.4 ppm. Aromatic protons were detected as multiplets in the region of δ 7.0-8.5 ppm. The ^{13}C NMR spectra showed signals for methylene and methine carbons of the pyrazoline ring at approximately δ 40 and δ 54 ppm, respectively, along with signals corresponding to carbonyl and thioamide carbons. Mass spectrometry further confirmed the structures by displaying molecular ion peaks consistent with theoretical values. For example, compound **Py1** (*m.f.* $C_{19}H_{14}N_3O_2SCl$) showed a molecular ion peak at *m/z* 392. Based on these results, the combined spectroscopic and analytical data confirmed the successful synthesis and structural integrity of the pyrazoline-based carbothioamide derivatives.

In silico and ADMET study

Homology modelling: Homology modelling was performed to find the missing residues in the protein structure to ensure the structural completeness of the EGFR kinase domain used in the docking studies. Fig. 3 shows the superimposed structures of the original EGFR protein and the homology-modelled structure, with the newly added residues highlighted. The green coloured segments represent the modelled regions reconstructed during the homology modelling process.

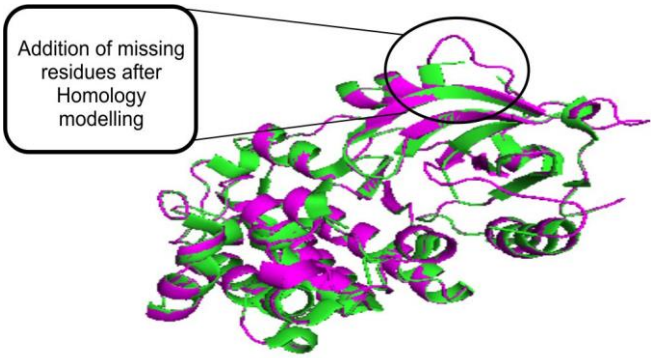

Fig. 3. Homology modelling of co-crystal ligand

This structural refinement was important to improve molecular docking accuracy by restoring the binding site's biologically relevant conformation. The co-crystallised ligand was retained to validate the modelled protein by ensuring its binding pose remained consistent, thereby confirming the reliability of the model for further *in silico* analyses.

Molecular docking: Molecular docking studies were performed to evaluate the binding affinities of the synthesised pyrazoline derivatives (**Py1-Py5**) against the EGFR kinase domain, utilizing the co-crystallised ligand (O3P) as a reference. The reference ligand O3P exhibited a docking score of -10.0 kcal/mol, while compound **Py3** demonstrated the highest binding affinity among the synthesized derivatives with a score of -10.2 kcal/mol. Other compounds also showed favourable docking scores including compound **Py1** (-9.4 kcal/mol), **Py5** (-9.3 kcal/mol), **Py2** (-9.1 kcal/mol) and **Py4** (-8.5 kcal/mol). These results indicate that all synthesized molecules possess the ability to interact effectively with the active site of EGFR (Table-1). The superior docking score of compound **Py3** may be attributed to its structural features that facilitate stronger interactions within the binding pocket, such as hydrophobic interactions, π–π stacking and hydrogen bonding. In addition, compound **Py2** displayed the lowest IC_{50} value (44.47 μg/ mL) against MCF-7 cells along with a favourable docking score (-9.1 kcal/mol), highlighting its potential as an effective EGFR inhibitor.

Protein–ligand interaction analysis: To examine the binding orientation and key molecular interactions within the EGFR active site, molecular docking studies were performed for the co-crystallized ligand (O3P) and the synthesized novel pyrazoline derivatives (**Py1-Py5**). The results (Fig. 4) indicate that all compounds established multiple hydrogen bonds and hydrophobic interactions with important amino acid residues located in the EGFR binding pocket. Compound **Py1** interacted through hydrogen bonding with Val31, Ala48, Thr95 and Lys50. Py2 formed interactions with Lys50, Thr95, Leu23 and Leu149, suggesting stable accommodation within the binding cavity. Compound **Py3**, which exhibited the highest docking score, showed strong interactions with Val31, Thr95, Lys50, Ala48, Met98 and Phe302, indicating a favourable binding orientation within the active site. Compound **Py4** interacted with residues such as Thr159, Leu23, Leu93 and Val31, whereas compound **Py5** formed hydrogen bond interactions with Thr95, Leu149, Gly24, Met98 and Val31.

For comparison, the reference ligand O3P interacted with Lys50, Thr95, Val31, Met98 and Leu97 within the EGFR active site. Remarkably, several residues including Lys50, Thr95, Val31 and Met98 were involved in the binding interactions of most compounds, suggesting their crucial role in stabilizing ligand binding. These observations highlight the ability of the synthesized derivatives to occupy the EGFR binding pocket effectively, supporting their potential as EGFR inhibitors. Although compound **Py3** demonstrated the strongest docking affinity, compound **Py2** showed the highest cytotoxic activity *in vitro*. This difference may arise from factors such as variations in membrane permeability, metabolic stability or interactions with additional cellular targets. While docking studies provide insight into the affinity of compounds toward the EGFR active site, the biological activity observed *in vitro* is also influenced by pharmacokinetic behaviour and cell-specific responses.

ADMET and synthetic accessibility analysis: In order to evaluate the synthesised compounds **Py1-Py5** for drug-likeness, physico-chemical properties and toxicity, an *in silico* ADMET evaluation was performed using SwissADME and associated tools. All compounds had molecular weights below the acceptable range (< 500 Da) according to Lipinski's rule of five, ranging from 383.86 (**Py1**) to 439.493 (**Py4**). Since **Py1** and **Py2** were slightly more lipophilic (3.84 and 3.74, respectively), the log P values for all compounds were in the ideal range (< 5), indicating adequate membrane permeability. The hydrogen bond acceptors (HBA) and hydrogen bond donors (HBD) of all compounds were in the drug-like range, indicating the possibility of favourable pharmacokinetics. All analogues scored 4/4, indicating that the compounds fulfilled the Lipinski criteria well and were therefore drug-like (Table-

TABLE-1
BINDING AFFINITY AND INTERACTION PROFILE OF THE **Py1-Py5** COMPOUNDS AND CO-CRYSTAL LIGAND O3P

Compounds	Binding energy (Kcal/mol)	Interacting amino acid residues
Py1	-9.4	Leu23 (Hydrogen bond)/Leu23, Val31, Ala48, Lys50, Leu93, Thr95, Leu149 (Hydrophobic)/Lys50 (Salt Bridges)
Py2	-9.1	Leu23, Ala48, Lys50, Leu93, Thr95, Leu149 (Hydrophobic)/Lys50 (Salt Bridges)
Py3	-10.2	Leu23 (Hydrogen bond)/Leu23, Val31, Ala48, Lys50, Leu93, Thr95, Leu149, Met98, Phe302 (Hydrophobic)/ Lys50 (Salt Bridges)
Py4	-8.5	Lys50 (Hydrogen bond), Leu23, Val31, Lys50, Leu82, Leu93, Thr95, Thr159 (Hydrophobic)
Py5	-9.3	Gly24, Met98Val31 (Hydrogen bond), Lys50, Leu93, Thr95, Leu149 (Hydrophobic)/Lys50 (Salt Bridges)
Co-crystal ligand	-10.0	Met98 (Hydrogen bond) Leu23, Val31, Lys50, Leu93, Thr95, Leu97, Leu163 (Hydrophobic)/Met71, Leu93, Thr95 (Halogen bonds)

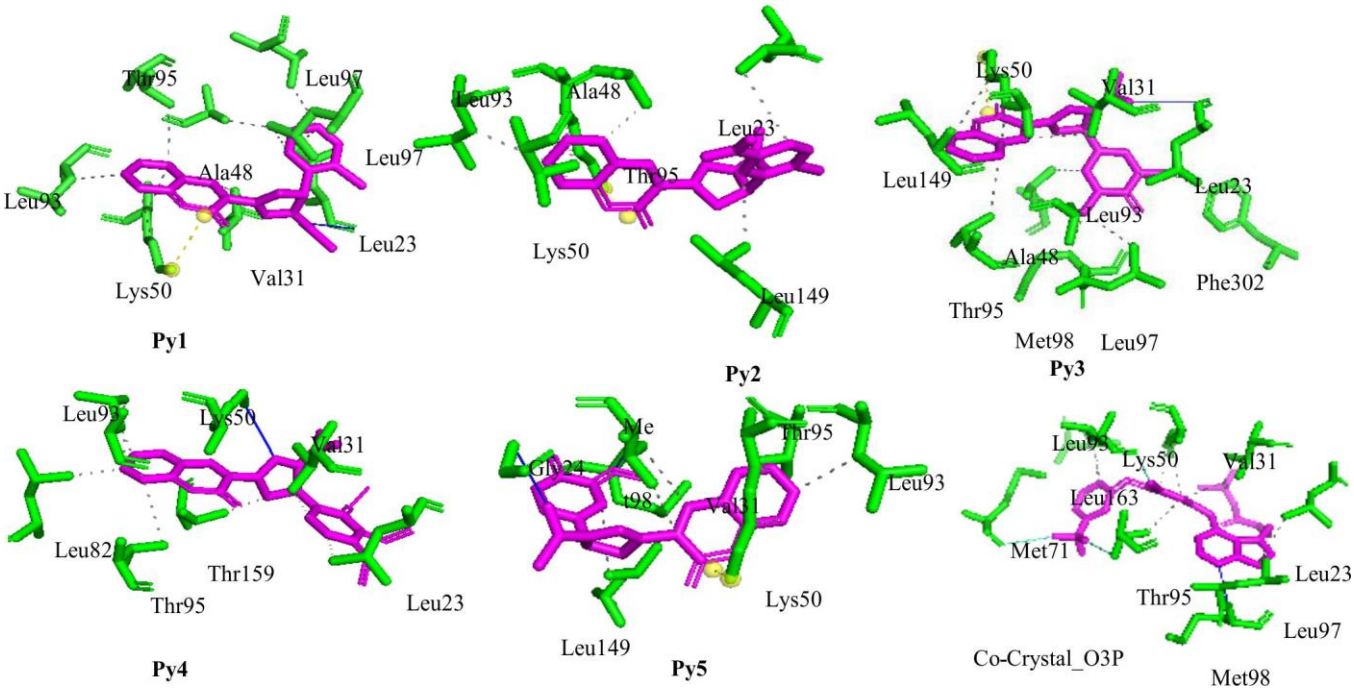

Fig. 4. Interactions of novel compounds **Py1**-**Py5** and co-crystal ligand O3P with protein EGFR kinase

TABLE-2
ADMET DATA OF COMPOUNDS **Py1**-**Py5** AND CO-CRYSTAL LIGAND

ADMET properties	**Py1**	**Py2**	**Py3**	**Py4**	**Py5**	CO-Crystal ligand O3P
MW	383.86	428.857	393.468	439.493	395.44	547.96
LogP	3.8411	3.7493	3.51014	3.2135	2.9019	5.9166
HBA	4	6	5	7	6	7
HBD	1	1	2	1	2	3
Lipinski	4	4	4	4	4	2
QED	0.53	0.29	0.51	0.47	0.51	0.24
TPSA	71.83	114.97	92.06	99.52	101.29	101.3
Ames	0.10	0.61	0.23	0.14	0.31	0.19
Bioavailability	0.85	0.86	0.89	0.91	0.82	0.800729
Carcinogenicity	0.30	0.34	0.38	0.20	0.13	78.32493
BBB	0.74	0.80	0.40	0.63	0.55	43.62156
ClinTox	0.04	0.09	0.05	0.06	0.06	1

MW = molecular weight, HBA = hydrogen bond acceptor, HBD = hydrogen bond donor, QED = quantitative estimation of drug likeliness, TPSA = topological polar surface area, Ames = AmesSalmonella/microsomemutagenicityassay, BBB = blood-brain barrier

2). The range of QED (quantitative estimate of drug-likeness) values was between 0.29 (**Py2**) and 0.53 (**Py1**), indicating a moderate to high potential for drug-likeness. The topological polar surface area (TPSA) values ranged from 71.83 $Å^2$ (**Py1**) to 114.97 $Å^2$ (**Py2**), indicating high oral bioavailability. It is noteworthy that none of the compounds exhibited significant Ames toxicity and all showed high bioavailability (> 0.80). Compounds **Py1** to **Py3** were predicted to penetrate the blood-brain barrier (BBB) into the central nervous system (CNS), although compounds **Py4** and **Py5** had moderate BBB values. Carcinogenicity projections ranged from 0.13 to 0.38, indicating low to insignificant risk for the synthesised compounds. However, the reference co-crystal O3P compound (75.99) had much higher ClinTox scores than this molecule, suggesting the relatively lesser toxicity (Table-2). SwissADME was also used to evaluate synthetic accessibility, which ranged from 4.04 (**Py1**) to 4.39 (**Py4**), indicating that the compounds are relatively easy to synthesise under typical laboratory conditions (Table-3). The combined *in silico* analysis shows that the synthesised pyrazoline-based coumarin derivatives (**Py1**-**Py5**) exhibit potential oral bioavailability, drug-likeness and synthetic feasibility, along with excellent physico-chemical and pharmacokinetic properties. These properties favour their further investigation as potential EGFR kinase inhibitors.

Biological evaluation: To determine the cytotoxic capability of the synthesised pyrazoline-based derivatives (**Py1**-**Py5**), the MTT test was utilised, with 5-fluorouracil (5-FU) acting as the reference standard. After incubating for 24 h, the IC_{50} values were calculated for a 10-100 µg/mL. As observed in the dose-response plot (Fig. 5), all compounds produced a concentration-dependent decrease in cell viability, confirming dose-dependent cytotoxic activity.

TABLE-3
SYNTHETIC ACCESSIBILITY SCORE VALUES OF COMPOUNDS **Py1-Py5**

Compounds	Synthetic accessibility score
Py1	4.04
Py2	4.08
Py3	4.18
Py4	4.39
Py5	4.10

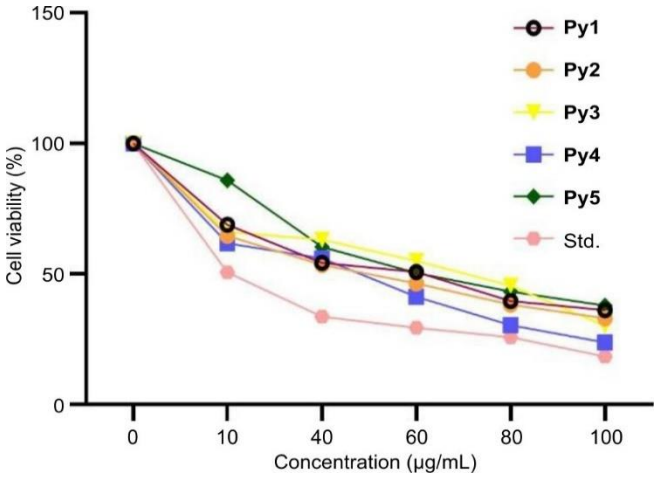

Fig. 5. Dose response curves showing the cell viability

The cytotoxic effects of the synthesised pyrazoline derivatives (**Py1-Py5**) were assessed by measuring percent cell viability across a concentration range (0-100 µg/mL) and the corresponding IC_{50} values are shown in Table-4. Among the studied concentrations, the standard anticancer drug 5-FU showed the highest potency (IC_{50} = 9.06 µg/mL) and the drastical reduction in viability. Compound **Py2** showed the highest potency (IC_{50} = 44.47 µg/mL) among the pyrazoline derivatives, which is consistent with its reduced percent viability at intermediate and high doses on the graph. **Py5** (IC_{50} = 61.07 µg/mL) and particularly **Py3** (IC_{50} = 90.93 µg/mL) were less potent, as seen by their comparatively higher percent viability at similar dosages, while **Py4** (IC_{50} = 50.09 µg/mL) and **Py1** (IC_{50} = 58.16 µg/mL) had moderate activity. A clear structure activity relationship among the series is suggested by the close match between the ordering of the viability curves and the IC_{50} ranking, which supports the dependability of the assay. These findings suggest that certain substituents in Py2 (and to a lesser extent **Py4**) may increase cytotoxic action; on the other hand, characteristics in **Py3** probably decrease cellular uptake or target engagement.

TABLE-4
CYTOTOXIC IC_{50} VALUES OF COMPOUNDS **Py1-Py5** AGAINST MCF7 CELL LINE

Sample	IC_{50} (µg/mL)
Control	–
Py1	58.16
Py2	44.47
Py3	90.93
Py4	50.09
Py5	61.07
5FU	9.06

Structural-activity relationship (SAR): The IC_{50} values and structural changes of the synthesised pyrazoline derivatives (**Py1-Py5**) were used to determine their structure activity relationship. The coumarin–pyrazoline core is shared by all compounds, but the cytotoxic effectiveness was greatly impacted by variations in the substituents on the aromatic rings. **Py2** was the most active of the series, indicating that the presence of an electron-withdrawing group, like a halogen on the aromatic ring, increases lipophilicity and promotes stronger interactions inside the binding pocket. **Py4** also shown good activity, which could be explained by the presence of methoxy groups that enhance molecule stability and have a mild impact on electron density. The moderate cytotoxicity of **Py1** and **Py5** suggests that their substituent patterns provide a compromise between polar and hydrophobic interactions. **Py3**, on the other hand, had the lowest activity, which may be because of the presence of large or potent electron-donating groups that lower cellular uptake and binding affinity. Based on these results, the trend **Py2** > **Py4** > **Py1** > **Py5** > **Py3** shows that cytotoxic activity is favoured by the addition of somewhat electron-withdrawing or less sterically hindered substituents, offering valuable information for additional structural optimisation of this pyrazoline scaffold.

Conclusion

In the present work, a series of coumarin-based pyrazoline derivatives (**Py1-Py5**) was successfully synthesized and characterized through IR, ^{1}H NMR, ^{13}C NMR and mass spectrometry analyses. The synthesized compounds were further evaluated for their anticancer potential against the MCF-7 breast cancer cell line, where all derivatives displayed significant cytotoxic activity. Among the tested compounds, **Py2** showed the most pronounced inhibitory effect with an IC_{50} value of 44.47 µg/mL, followed by **Py4**, **Py1** and **Py5**. Molecular docking analysis supported the experimental findings by demonstrating favourable interactions of the compounds within the EGFR kinase binding site. In particular, compound **Py2** exhibited strong binding affinity (-9.3 kcal/mol), indicating its potential to interact effectively with the EGFR active site. The computational ADMET predictions and synthetic accessibility evaluation suggested that the designed molecules possess acceptable pharmacokinetic properties, relatively low toxicity risks and feasible synthetic profiles. The presence of the 2-chloro-5-nitro substituent in compound **Py2** appears to contribute significantly to its enhanced biological activity, highlighting its importance in the structure-activity relationship within this series. These findings suggest that coumarin–pyrazoline hybrids represent promising scaffolds for the development of EGFR-targeted anticancer agents.

ACKNOWLEDGEMENTS

The researchers express their gratitude to Rashtrasant Tukadoji Maharaj Nagpur University Nagpur, Department of Pharmaceutical Sciences, for their support of this research.

CONFLICT OF INTEREST

The authors declare that there is no conflict of interests regarding the publication of this article.

DECLARATION OF AI-ASSISTED TECHNOLOGIES

During the preparation of this manuscript, the authors used an AI-assisted tool(s) to improve the language. The authors reviewed and edited the content and take full responsibility for the published work.

REFERENCES

1. M. Hossain, *Sci. J. Chem.*, **6**, 83 (2018); https://doi.org/10.11648/j.sjc.20180605.12
2. M.M. Fakhry, K. Mahmoud, M.S. Nafie, A.O. Noor, R.H. Hareeri, I. Salama and S.M. Kishk, *Pharmaceuticals*, **15**, 1245 (2022); https://doi.org/10.3390/ph15101245
3. T.D. Wahyuningsih, A.A.T. Suma and E. Astuti, *J. Appl. Pharm. Sci.*, **9**, 14 (2019); https://doi.org/10.7324/JAPS.2019.90303
4. N. Sharma, A. Kumar, V.P. Verma, M.B. Singh, P. Singh and R. Shrivastava, *RSC Adv.*, **15**, 48529 (2025); https://doi.org/10.1039/D5RA06322A
5. A.L. Kerek, L. Kozan, G.S. Fonseca, B.S. dos Santos, R.P. Guaringue, L. Sens and B.C. Fiorin, *Orbital: Electron. J. Chem.*, **17**, 234 (2025); https://doi.org/10.17807/orbital.v17i2.21049
6. A. Tiwari, A. Bendi and A.S. Bhathiwal, *ChemistrySelect*, **6**, 12757 (2021); https://doi.org/10.1002/slct.202103779
7. P. Rani, S. Dhillon, G. Kumari, M. Chahal, D.K. Aneja, B. Pareek and M. Kinger, *Bull. Korean Chem. Soc.*, **46**, 481 (2025); https://doi.org/10.1002/bkcs.70022
8. H.N. Hafez, H.Y. Otaif, B.H. Alshammari, N.S. Alhebshe, A.F. El-Sayed, H.-A.S. Abbas and R.A. Ammar, *Sci. Rep.*, **16**, 7931 (2026); https://doi.org/10.1038/s41598-026-38237-9
9. R.A. Weinberg and R.A. Weinberg, The Biology of Cancer, W.W. Norton & Company, New York, USA (2006).
10. C. Mattiuzzi and G. Lippi, *Epidemiol. Glob. Health*, **9**, 217 (2019); https://doi.org/10.2991/jegh.k.191008.001
11. R.L. Siegel, K.D. Miller and A. Jemal, *CA Cancer J. Clin.*, **70**, 7 (2020); https://doi.org/10.3322/caac.21590
12. B.E. Wilson, R. Sullivan, R. Peto, B. Abubakar, C. Booth, G. Werutsky, C. Adams, A. Saint-Raymond, T.R. Fleming, K. Lyerly and J.R. Gralow, *JCO Glob. Oncol.*, **9**, e2300294 (2023); https://doi.org/10.1200/GO.23.00294
13. S.U. Khan, K. Fatima, S. Aisha and F. Malik, *Cell Commun. Signal.*, **22**, 109 (2024); https://doi.org/10.1186/s12964-023-01302-1
14. A. Saini, M. Kumar, S. Bhatt, V. Saini and A. Malik, *Int. J. Pharm. Sci. Res.*, **11**, (2020); https://doi.org/10.13040/ijpsr.0975-8232.11(7).3121-34
15. H.-Y. Min and H.-Y. Lee, *Exp. Mol. Med.*, **54**, 1670 (2022); https://doi.org/10.1038/s12276-022-00864-3
16. T. Yamaoka, S. Kusumoto, K. Ando, M. Ohba and T. Ohmori, *Int. J. Mol. Sci.*, **19**, 3491 (2018); https://doi.org/10.3390/ijms19113491
17. A.W. Burgess, *Growth Factors*, **26**, 263 (2008); https://doi.org/10.1080/08977190802312844
18. Z. Wang, *Methods Mol. Biol.*, **1652**, 3 (2017); https://doi.org/10.1007/978-1-4939-7219-7_1
19. R. Roskoski Jr., *Pharmacol. Res.*, **79**, 34 (2014); https://doi.org/10.1016/j.phrs.2013.11.002
20. X. Liu, P. Wang, C. Zhang and Z. Ma, *Oncotarget*, **8**, 50209 (2017); https://doi.org/10.18632/oncotarget.16854
21. R. Qureshi, B. Zou, T. Alam, J. Wu, V.H.F. Lee and H. Yan, *IEEE/ACM Trans. Comput. Biol. Bioinformatics*, **20**, 238 (2023); https://doi.org/10.1109/TCBB.2022.3141697
22. K. Zhang and Q. Yuan, *J. Cancer Res. Therap.*, **12S**, C131 (2016); https://doi.org/10.4103/0973-1482.200613
23. T. Zubair and D. Bandyopadhyay, *Int. J. Mol. Sci.*, **24**, 2651 (2023); https://doi.org/10.3390/ijms24032651
24. E. Mansour, I.F. Nassar, A.A.I. Mekawey and S.I. Elewa, *Russ. J. Bioorg. Chem.*, **46**, 382 (2020); https://doi.org/10.1134/S1068162020030061
25. M.I. Chouiter, H. Boulebd, D.M. Pereira, P. Valentão, P.B. Andrade, A. Belfaitah and A.M.S. Silva, *Future Med. Chem.*, **12**, 493 (2020); https://doi.org/10.4155/fmc-2019-0342
26. V.S. Suryawanshi, S.P. Pawar, M.S. Kolpe, H.T.M. Abdelghani, S. Chikhale, P.C. Patil and S. Bhowmick, *Struct. Chem.*, **36**, 681 (2025); https://doi.org/10.1007/s11224-024-02397-z
27. R.J. Bienstock, *Methods Mol. Biol.*, **1289**, 119 (2015); https://doi.org/10.1007/978-1-4939-2486-8_10
28. H. Deka, A.D. Pawar, M.S. Battula, G.E. Eldesoky, O.D. Shinde, P.C. Patil, T.K. Mistri, H.V. Shahare and S. Bhowmick, *J. Mol. Liq.*, **411**, 125782 (2024); https://doi.org/10.1016/j.molliq.2024.125782
29. AutoDockTools–AutoDock Suite, Available online: https://autodocksuite.scripps.edu/adt/
30. K. Aertgeerts, R. Skene, J. Yano, B.-C. Sang, H. Zou, G. Snell, A. Jennings, K. Iwamoto, N. Habuka, A. Hirokawa, T. Ishikawa, T. Tanaka, H. Miki, Y. Ohta and S. Sogabe, *J. Biol. Chem.*, **286**, 18756 (2011); https://doi.org/10.1074/jbc.M110.206193
31. A. Waterhouse, M. Bertoni, S. Bienert, G. Studer, F.T. Heer, G. Tauriello, R. Gumienny, T.A.P. de Beer, C. Rempfer, L. Bordoli, R. Lepore and T. Schwede, *Nucleic Acids Res.*, **46(no. W1)**, W296 (2018); https://doi.org/10.1093/nar/gky427
32. Y.N. Nayak, S. Pandey, S.R. Pai, N.S. Gandhi, R. Nayak, V. Pandey, Z. Xi, B. Basappa and S.L. Gaonkar, *J. Mol. Struct.*, **1324**, 140821 (2025); https://doi.org/10.1016/j.molstruc.2024.140821
33. R.V. Chikhale, H.T.M. Abdelghani, H. Deka, A.D. Pawar, P.C. Patil and S. Bhowmick, *Comput. Biol. Chem.*, **110**, 108034 (2024); https://doi.org/10.1016/j.compbiolchem.2024.108034
34. R.V. Chikhale, G.E. Eldesoky, M.S. Kolpe, V.S. Suryawanshi, P.C. Patil and S. Bhowmick, *Heliyon*, **10**, e26802 (2024); https://doi.org/10.1016/j.heliyon.2024.e26802
35. A. Daina, O. Michielin and V. Zoete, *Sci. Rep.*, **7**, 42717 (2017); https://doi.org/10.1038/srep42717
36. F. En-Nahli, H. Hajji, M. Ouabane, M. Aziz-Ajana, C. Sekatte, T. Lakhlifi and M. Bouachrine, *Arab. J. Chem.*, **16**, 105262 (2023); https://doi.org/10.1016/j.arabjc.2023.105262
37. A. Abu-Hashem, O. Hakami and N. Amri, *Heliyon*, **10**, e26735 (2024); https://doi.org/10.1016/j.heliyon.2024.e26735
38. R.F. George, E.M. Samir, M.N. Abdelhamed, H.A. Abdel-Aziz and S.E.-S. Abbas, *Bioorg. Chem.*, **83**, 186 (2019); https://doi.org/10.1016/j.bioorg.2018.10.038